Estimation of elastic constants in HTI media using Gauss-Newton and Full-Newton multi-parameter full waveform inversion

Wenyong Pan, Kristopher A. Innanen, Gary F. Margrave, CREWES Project, Univ. of Calgary, Michael C. Fehler, ERL, M.I.T, Xinding Fang, M.I.T, currently Chevron Energy Technology Company, and Junxiao Li, CREWES Project, Univ. of Calgary*

SUMMARY

We consider the estimation of the elastic constants of a fractured medium, using multi-parameter FWI and modeling naturally fractured reservoirs as equivalent anisotropic media. Multi-parameter FWI remains exposed to a range of challenges, one of which being the cross-talk problem resulting from overlap of Fréchet derivative wavefields. Cross-talk is strongly influenced by the form of the scattering patterns for each parameter, i.e., the relative strength of incoming to outgoing waves from a volume scattering element as a function of opening angle. In the numerical section, we illustrate the analytic and numerical scattering patterns of different elastic constants in HTI media for cross-talk analysis. We also analyze the role of multi-parameter approximate Hessian in suppressing cross-talk. The gradient vectors are also contaminated by the doubly-scattered energy in the data residuals. The second-order term in the Hessian, which we construct using the adjoint-state technique, can suppress the multi-parameter second-order scattering effects in the gradient. We apply Gauss-Newton and Full-Newton multi-parameter FWI on several numerical examples to verify multi-parameter Hessian's role in suppressing cross-talk and second-order scattering effects.

INTRODUCTION

The influence of fractures/cracks in a geological medium on the seismic response can be modelled via an equivalent anisotropic solid and the associated elastic stiffness coefficients c_{IJ} (Hudson, 1981; Schoenberg, 1983). In reflection seismology, most current methods for estimation of fracture information focus on amplitude and travel-time methods (Thomsen, 1988; Tsvankin, 1997). Full waveform inversion (FWI) uses full wavefield information to estimate subsurface properties by iteratively minimizing the difference between modelled and observed data (Lailly, 1983; Tarantola, 1984; Virieux and Operto, 2009; Warner et al., 2013). In this research, we consider the problem of estimation of the elastic constants in anisotropic media using multi-parameter FWI.

Much current FWI research emphasizes reconstruction of the P-wave velocity, and associated core problems such as cycle-skipping (Ma and Hale, 2012; Warner and Guasch, 2014; Wu et al., 2014; Yao et al., 2014). Inverting multiple parameters using multi-parameter FWI has also, however, received increased attention in recent years, though it is a more challenging task. Involving several parameters increases the non-linearity of the inversion process and furthermore introduces parameter cross-talk, the conflation of the influence of one physical property on the data with another (Operto et al., 2013; Prieux et al., 2013; Innanen, 2014a). The parameter cross-talk arises in steepest-descent method, wherein update in each parameter proceed with no accounting for multi-parameter character of the problem. Tarantola (1986) originally introduced the scattering patterns for cross-talk analysis of different parameter classes. The scattering patterns of different parameter classes in anisotropic media have been studied by many researchers (Gholami et al., 2013; Alkhalifah and Plessix, 2014). Pan et al. (2014a) derived the analytic expressions of 3D scattering patterns for the elastic constants in general anisotropic media. Here we use them to analyze the cross-talk problem when inversing the elastic constants in HTI media.

The multi-parameter Hessian is a square and symmetric matrix with a block structure. For the approximate Hessian associated with a multi-parameter Gauss-Newton update, off-diagonal blocks measure correlation of Fréchet derivative wavefields with respect to different physical parameters, and they act to mitigate the coupling effects. Innanen (2014b,a), for instance, showed that the diagonal elements internal to the off-diagonal blocks suppress cross-talk, in precritical reflection FWI, in a manner precisely consistent with AVO inversion and linearized inverse scattering. In this research, we numerically examine the ability of the multi-parameter approximate Hessian to suppress cross-talk in HTI parameters estimation.

The gradient vector is also known to be contaminated by second-order scattered energy in the data residuals. Pratt et al. (1998) discussed and analyzed the second-order term in mono-parameter full Hessian, which accounts for the second-order scattering effects. This term becomes important when the data residuals or the second-order scattered energy are very strong. Incorporating this second-order term can eliminate the second-order scattering effects in the gradient vector. Here we include this second-order term, employing an adjoint-state method to calculate it. We organize our results as follows. First, we review the theories for forward modelling and multi-parameter FWI. We then quantitatively discuss cross-talk in multi-parameter FWI and the role of multi-parameter Hessian in suppressing cross-talk and second-order scattering effects, and describe how to construct the second-order term using adjoint-state method. In the numerical modelling section, we verify the analytic results of the scattering patterns using a 2D numerical example and discuss the cross-talk problem for elastic constants inversion in HTI media. We then exemplify the Gauss-Newton and Full-Newton FWI using numerical examples.

THEORY AND METHODS

Forward Modelling Problem

We consider media containing parallel vertical fractures, which can be described by elastic stiffness coefficients c_{IJ} (Hudson, 1981). The equation of motion in general anisotropic and elastic media is expressed as:

$$\frac{\partial \sigma_{ij}}{\partial x_j} + f_i = \rho \frac{\partial^2 u_i}{\partial t^2}, \tag{1}$$

where $u_i(\mathbf{r},t)$ indicates particle displacement at Cartesian coordinate position $\mathbf{r} = (x,y,z)$ and time t, $f_i(\mathbf{r}_s)$ is the force term at position $\mathbf{r}_s$, ρ is the density and σ_{ij} denotes the stress tensor, which can be defined using Hooke's law,$\sigma_{ij} = c_{ijkl}e_{kl}$, where c_{ijkl} indicates the elastic modulus tensor, $e_{kl} = 1/2\left(\frac{\partial u_k}{\partial l} + \frac{\partial u_l}{\partial k}\right)$ is the strain tensor and the subscripts i, j, k and l take on the values of x, y, z (or 1, 2, 3). Because of the symmetry of the stress and strain tensors, the tensor c_{ijkl} can be represented more compactly using symmetric matrix c_{IJ} following Voigt recipe for indexes, where I and J range from 1 to 6 (Crampin, 1984).

Models containing parallel vertical fractures are equivalent to HTI medium, which can be characterized by 5 independent elastic constants $c_{33}, c_{55}, c_{11}, c_{13}, c_{44}$. We extract the x-z plane with zero azimuth angle from 3D geometry, which forms the simplified 2D HTI model described by 4 elastic constants (c_{33}, c_{55}, c_{11} and c_{13}). Numerical solutions of the wavefields are calculated using an explicit finite-difference method with fourth-order accuracy in space and second-order accuracy in time (Virieux, 1986; Levander, 1988). A non-splitting perfectly matched layer (NPML) boundary condition is applied on all boundaries of the model (Berenger, 1994; Wang and Tang, 2003).

Elastic constants estimation in HTI media using multi-parameter FWI

Multi-parameter Gauss-Newton and Full-Newton FWI

Review of Least-squares Waveform Inversion

In FWI subsurface properties are estimated through an iterative process by minimizing the difference between synthetic data $\mathbf{u}_{syn}$ and observed data $\mathbf{u}_{obs}$ (Lailly, 1983; Tarantola, 1984; Virieux and Operto, 2009). The misfit function Φ is formulated in a least-squares form:

$$\Phi(\mathbf{m}(\mathbf{r})) = \frac{1}{2}\sum_{\mathbf{r}_s}\sum_{\mathbf{r}_g}\sum_{\omega}\|\mathbf{u}_{obs}(\mathbf{r}_g,\mathbf{r}_s,\omega)-\mathbf{u}_{syn}(\mathbf{r}_g,\mathbf{r}_s,\omega)\|^2, \quad (2)$$

where $\mathbf{m}$ indicates the model parameter vector, $\mathbf{r}_s$ and $\mathbf{r}_g$ respectively denote the positions of sources and receivers, ω is angular frequency, and $\|\cdot\|$ means the ℓ-2 norm. Within Newton optimization framework, the model perturbation can be constructed by the gradient vector $\mathbf{g}$ and inverse Hessian operator $\mathbf{H}^{-1}$ (Virieux and Operto, 2009):

$$\delta\mathbf{m}_n = -\mu\mathbf{H}^{-1}\mathbf{g}, \quad (3)$$

where μ is the step length. The gradient is the first-order partial derivative of the misfit function with respect to the model parameter and it can be constructed by convolution between the Jacobian matrix with complex conjugate of the data residuals $\Delta\mathbf{d}$:

$$\mathbf{g} = \sum_{\mathbf{r}_s}\sum_{\mathbf{r}_g}\sum_{\omega}\Re\left(\mathbf{J}^{\dagger}\Delta\mathbf{d}^{*}(\mathbf{r}_g,\mathbf{r}_s,\omega)\right), \quad (4)$$

where "$\dagger$" indicates transpose, "$*$" means complex conjugate, $\Re(\cdot)$ denotes the real part and $\mathbf{J}$ is the Jacobian matrix $\mathbf{J} = \partial\mathbf{u}(\mathbf{r}_g,\mathbf{r}_s,\omega)/\partial\mathbf{m}$. To avoid the direct calculation of the Jacobian matrix, the adjoint-state method is always used by cross-correlating the forward modelled wavefields and backpropagated wavefields (Lailly, 1983; Tarantola, 1984; Mora, 1987). The gradient is then expressed as:

$$\mathbf{g} = \sum_{\mathbf{r}_s}\sum_{\mathbf{r}_g}\sum_{\omega}\Re\left(\tilde{\mathbf{f}}^{\dagger}\left(\mathbf{L}^{-1}\right)^{\dagger}\Delta\mathbf{d}^{*}(\mathbf{r}_g,\mathbf{r}_s,\omega)\right), \quad (5)$$

where $\tilde{\mathbf{f}} = -(\partial\mathbf{L}/\partial\mathbf{m})\mathbf{u}$ is the virtual source term and $\mathbf{L}$ is the impedance matrix. The gradient is contaminated by spurious correlations because of band-limited seismic data and it is also poorly-scaled as the result of geometrical spreading and uneven subsurface illumination.

The full Hessian is the second-order partial derivative of the misfit function with respect to the model parameter:

$$\mathbf{H} = \frac{\partial^2\Phi}{(\partial\mathbf{m})^2} = \sum_{\mathbf{r}_s}\sum_{\mathbf{r}_g}\sum_{\omega}\Re\left(\mathbf{J}^{\dagger}\mathbf{J}^{*} + \left(\frac{\partial\mathbf{J}}{\partial\mathbf{m}}\right)^{\dagger}\Delta\mathbf{d}^{*}(\mathbf{r}_g,\mathbf{r}_s,\omega)\right), \quad (6)$$

where the first term $\mathbf{J}^{\dagger}\mathbf{J}^{*}$ indicates the correlation of two Fréchet derivative wavefields and it accounts for the first-order scattering effects. Used alone, it forms the approximate Hessian $\tilde{\mathbf{H}}$ associated with Gauss-Newton methods. The Gauss-Newton approximate Hessian is diagonally dominant and banded, which allows it to remove the finite frequency effects in the gradient (Pratt et al., 1998). Moreover, the gradient is also contaminated by the second-order scattering artifacts, which can be mitigated by the second term $\bar{\mathbf{H}}$ in equation (6) constructed by the correlation of the second-order partial derivative wavefields with the complex conjugate of data residuals.

Simultaneous Multi-parameter Updates

When considering simultaneous multi-parameter updates, as for the 2D HTI case, the model perturbation and gradient vectors are:

$$\begin{aligned}\delta\mathbf{m} &= \begin{bmatrix}\delta\mathbf{c}_{33} & \delta\mathbf{c}_{55} & \delta\mathbf{c}_{11} & \delta\mathbf{c}_{13}\end{bmatrix}^{\dagger},\\ \mathbf{g} &= \begin{bmatrix}\mathbf{g}_{33} & \mathbf{g}_{55} & \mathbf{g}_{11} & \mathbf{g}_{13}\end{bmatrix}^{\dagger},\end{aligned} \quad (7)$$

where $\delta\mathbf{c}_{33}$, $\delta\mathbf{c}_{55}$, $\delta\mathbf{c}_{11}$ and $\delta\mathbf{c}_{13}$ are the model perturbation vectors for the 4 elastic constants and $\mathbf{g}_{33}$, $\mathbf{g}_{55}$, $\mathbf{g}_{11}$ and $\mathbf{g}_{13}$ are the gradient vectors corresponding to different elastic constants. These gradient vectors are constructed by convolution between Fréchet derivative wavefields and complex conjugate of the data residuals. Consider, for instance, the gradient vector $\mathbf{g}_{33}$ for c_{33}:

$$\mathbf{g}_{33} = \sum_{\mathbf{r}_s}\sum_{\mathbf{r}_g}\sum_{\omega}\Re\left(\mathbf{J}_{33}^{\dagger}\Delta\mathbf{d}^{*}(\mathbf{r}_g,\mathbf{r}_s,\omega)\right), \quad (8)$$

where $\mathbf{J}_{33}$ indicates the Fréchet derivative wavefields due to c_{33}. Gradient vector $\mathbf{g}_{33}$ has no internal mechanism for determining which, if any, of the variations in the residuals are due to c_{33}, and which are due the other three parameters. The resulting confusion experienced by steepest-descent update is known as the parameter cross-talk. Furthermore, the gradient vector also suffers from doubly-scattered energy in data residuals.

The multi-parameter Hessian has a block structure. The 2D subsurface model contains N_xN_z nodes, and N_p independent physical parameters are assigned to describe each node. The multi-parameter full Hessian thus is a $N_xN_zN_p \times N_xN_zN_p$ square and symmetric matrix, with N_p diagonal blocks and $N_p(N_p-1)$ off-diagonal blocks with each block a $N_xN_z \times N_xN_z$ square matrix. Hence, the full multi-parameter Hessian matrix $\mathbf{H}$ for the 2D HTI case has 16 block sub-matrices (N_p=4). Its Gauss-Newton approximation $\tilde{\mathbf{H}}$ can be expressed as:

$$\tilde{\mathbf{H}} = \begin{bmatrix}\tilde{\mathbf{H}}_{3333} & \tilde{\mathbf{H}}_{3355} & \tilde{\mathbf{H}}_{3311} & \tilde{\mathbf{H}}_{3313}\\ \tilde{\mathbf{H}}_{5533} & \tilde{\mathbf{H}}_{5555} & \tilde{\mathbf{H}}_{5511} & \tilde{\mathbf{H}}_{5513}\\ \tilde{\mathbf{H}}_{1133} & \tilde{\mathbf{H}}_{1155} & \tilde{\mathbf{H}}_{1111} & \tilde{\mathbf{H}}_{1113}\\ \tilde{\mathbf{H}}_{1333} & \tilde{\mathbf{H}}_{1355} & \tilde{\mathbf{H}}_{1311} & \tilde{\mathbf{H}}_{1313}\end{bmatrix}, \quad (9)$$

where the subscripts of the sub-block matrices in equation (9) correspond to two elastic constants be correlated. The Gauss-Newton approximation only accounts for the first-order scattering effects. When correlating the Fréchet derivative wavefields with the data residuals, doubly-scattered energy in the data residuals will result in gradient artifacts. The second-order term in full Hessian works as a de-multiple operator for suppressing some of these artifacts (Pratt et al., 1998). We will include this second-order term $\bar{\mathbf{H}}$ as an additional block matrix for HTI multi-parameter inversion:

$$\bar{\mathbf{H}} = \begin{bmatrix}\frac{\partial\mathbf{J}_{33}^{\dagger}}{\partial\mathbf{c}_{33}} & \frac{\partial\mathbf{J}_{33}^{\dagger}}{\partial\mathbf{c}_{55}} & \frac{\partial\mathbf{J}_{33}^{\dagger}}{\partial\mathbf{c}_{11}} & \frac{\partial\mathbf{J}_{33}^{\dagger}}{\partial\mathbf{c}_{13}}\\ \frac{\partial\mathbf{J}_{55}^{\dagger}}{\partial\mathbf{c}_{33}} & \frac{\partial\mathbf{J}_{55}^{\dagger}}{\partial\mathbf{c}_{55}} & \frac{\partial\mathbf{J}_{55}^{\dagger}}{\partial\mathbf{c}_{11}} & \frac{\partial\mathbf{J}_{55}^{\dagger}}{\partial\mathbf{c}_{13}}\\ \frac{\partial\mathbf{J}_{11}^{\dagger}}{\partial\mathbf{c}_{33}} & \frac{\partial\mathbf{J}_{11}^{\dagger}}{\partial\mathbf{c}_{55}} & \frac{\partial\mathbf{J}_{11}^{\dagger}}{\partial\mathbf{c}_{11}} & \frac{\partial\mathbf{J}_{11}^{\dagger}}{\partial\mathbf{c}_{13}}\\ \frac{\partial\mathbf{J}_{13}^{\dagger}}{\partial\mathbf{c}_{33}} & \frac{\partial\mathbf{J}_{13}^{\dagger}}{\partial\mathbf{c}_{55}} & \frac{\partial\mathbf{J}_{13}^{\dagger}}{\partial\mathbf{c}_{11}} & \frac{\partial\mathbf{J}_{13}^{\dagger}}{\partial\mathbf{c}_{13}}\end{bmatrix}\Delta\mathbf{d}^{*}, \quad (10)$$

whose elements are constructed by correlating the second-order partial derivative wavefields with the complex conjugate of the data residuals. For instance, the off-diagonal block $(\partial\mathbf{J}_{33}^{\dagger}/\partial\mathbf{c}_{55})\Delta\mathbf{d}^{*}$ accounts for the second-order partial derivative wavefields $\partial^2\mathbf{u}/(\partial\mathbf{c}_{33}\partial\mathbf{c}_{55})$.

To calculate this second-order preconditioner explicitly, $(N_pN_xN_z)^2/2$ forward modelling problems need to be solved, which is prohibitively expensive. By taking partial derivative with respect to model parameter $\mathbf{m}_1$ on both sides of wave equation gives:

$$\mathbf{L}\frac{\partial\mathbf{u}}{\partial\mathbf{m}_1} = -\frac{\partial\mathbf{L}}{\partial\mathbf{m}_1}\mathbf{u}. \quad (11)$$

On the right hand side of equation (11), the interaction of the incident wavefields with the model perturbation serves as first-order virtual source $\tilde{\mathbf{f}}$. Isolating the first-order partial derivative wavefields yields:

$$\frac{\partial\mathbf{u}}{\partial\mathbf{m}_1} = \mathbf{L}^{-1}\tilde{\mathbf{f}}. \quad (12)$$

Taking partial derivative with respect to different physical parameter $\mathbf{m}_2$ on both sides of equation (12) gives the equation describing the propagation of second-order scattered wavefields:

$$\mathbf{L}\frac{\partial^2\mathbf{u}}{\partial\mathbf{m}_1\partial\mathbf{m}_2} = \tilde{\tilde{\mathbf{f}}}_{\mathbf{m}_1\mathbf{m}_2}, \quad (13)$$

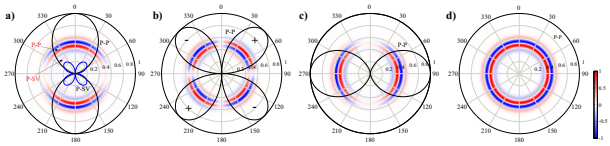

Figure 1: (a), (b), (c) and (d) show the analytic and numerical results of the P-P scattering patterns due to δc_{33}, δc_{55}, δc_{11} and δc_{13}.

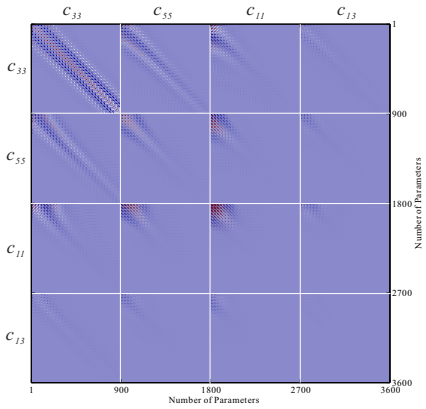

Figure 2: The multi-parameter approximate Hessian $\tilde{\mathbf{H}}$ (equation (9)) for elastic constants c_{33}, c_{55}, c_{11} and c_{13}.

where $\tilde{\tilde{\mathbf{f}}}_{\mathbf{m}_1\mathbf{m}_2}$ indicates the multi-parameter second-order virtual source:

$$\tilde{\tilde{\mathbf{f}}}_{\mathbf{m}_1\mathbf{m}_2} = -\frac{\partial \mathbf{L}}{\partial \mathbf{m}_1}\frac{\partial \mathbf{u}}{\partial \mathbf{m}_2} - \frac{\partial \mathbf{L}}{\partial \mathbf{m}_2}\frac{\partial \mathbf{u}}{\partial \mathbf{m}_1} - \frac{\partial^2 \mathbf{L}}{\partial \mathbf{m}_1 \partial \mathbf{m}_2}\mathbf{u}. \qquad (14)$$

It is also possible for us to calculate the second-order preconditioner for multi-parameter FWI using adjoint-state technique. Isolating the multi-parameter second-order partial derivative wavefields in equation (13) and substituting it into one sub-block of the second-order term gives:

$$\bar{\mathbf{H}}_{\mathbf{m}_1\mathbf{m}_2} = \sum_{\mathbf{r}_s}\sum_{\mathbf{r}_g}\sum_{\omega} \Re\left(\tilde{\tilde{\mathbf{f}}}^{\dagger}_{\mathbf{m}_1\mathbf{m}_2}\left(\mathbf{L}^{-1}\right)^{\dagger}\Delta\mathbf{d}^{*}(\mathbf{r}_g,\mathbf{r}_s,\omega)\right). \qquad (15)$$

Thus, the elements in the second-order term $\bar{\mathbf{H}}$ can also be calculated using adjoint-state method and additional $N_p N_x N_z$ forward modelling simulations are required. The multi-parameter second-order preconditioner shown in equation (10) is expressible as:

$$\bar{\mathbf{H}} = \begin{bmatrix} \tilde{\tilde{\mathbf{f}}}^{\dagger}_{c_{33}c_{33}} & \tilde{\tilde{\mathbf{f}}}^{\dagger}_{c_{33}c_{55}} & \tilde{\tilde{\mathbf{f}}}^{\dagger}_{c_{33}c_{11}} & \tilde{\tilde{\mathbf{f}}}^{\dagger}_{c_{33}c_{13}} \\ \tilde{\tilde{\mathbf{f}}}^{\dagger}_{c_{55}c_{33}} & \tilde{\tilde{\mathbf{f}}}^{\dagger}_{c_{55}c_{55}} & \tilde{\tilde{\mathbf{f}}}^{\dagger}_{c_{55}c_{11}} & \tilde{\tilde{\mathbf{f}}}^{\dagger}_{c_{55}c_{13}} \\ \tilde{\tilde{\mathbf{f}}}^{\dagger}_{c_{11}c_{33}} & \tilde{\tilde{\mathbf{f}}}^{\dagger}_{c_{11}c_{55}} & \tilde{\tilde{\mathbf{f}}}^{\dagger}_{c_{11}c_{11}} & \tilde{\tilde{\mathbf{f}}}^{\dagger}_{c_{11}c_{13}} \\ \tilde{\tilde{\mathbf{f}}}^{\dagger}_{c_{13}c_{33}} & \tilde{\tilde{\mathbf{f}}}^{\dagger}_{c_{13}c_{55}} & \tilde{\tilde{\mathbf{f}}}^{\dagger}_{c_{13}c_{11}} & \tilde{\tilde{\mathbf{f}}}^{\dagger}_{c_{13}c_{13}} \end{bmatrix} \left(\mathbf{L}^{-1}\right)^{\dagger}\Delta\mathbf{d}^{*}. \qquad (16)$$

To calculate this second-order preconditioner, we need an additional $4N_xN_z$ forward modelling simulations.

NUMERICAL EXPERIMENTS

Here we first numerically examine the scattering patterns of the elastic constants associated with a 2D HTI model. The calculations are done using an isotropic-elastic background model. The elastic constants are perturbed by 10% perturbations at the center of the model. One source

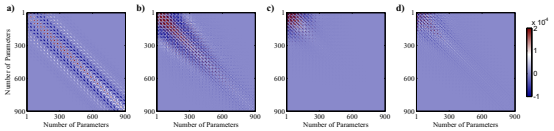

Figure 3: (a), (b), (c) and (d) show the diagonal blocks $\tilde{\mathbf{H}}_{3333}$, $\tilde{\mathbf{H}}_{5555}$, $\tilde{\mathbf{H}}_{1111}$ and $\tilde{\mathbf{H}}_{1313}$ of the multi-parameter approximate Hessian.

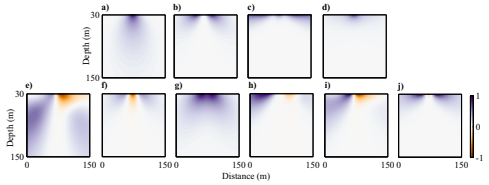

Figure 4: (a), (b), (c), (d), (e), (f), (g), (h), (i) and (j) show the diagonal elements in blocks $\tilde{\mathbf{H}}_{3333}$, $\tilde{\mathbf{H}}_{5555}$, $\tilde{\mathbf{H}}_{1313}$, $\tilde{\mathbf{H}}_{1111}$, $\tilde{\mathbf{H}}_{3355}$, $\tilde{\mathbf{H}}_{3311}$, $\tilde{\mathbf{H}}_{3313}$, $\tilde{\mathbf{H}}_{1111}$,$\tilde{\mathbf{H}}_{5511}$, $\tilde{\mathbf{H}}_{5513}$, and $\tilde{\mathbf{H}}_{1311}$.

is located at top left corner of the model. The incident P-wave is characterized by an inclination angle ϑ away from z-axis and an azimuthal angle φ away from x-axis. The scattered wave is characterized by corresponding angles θ and ϕ respectively.

The bold-black curves in Figure 1a, b, c and d show the analytic results of P-P scattering patterns due to δc_{33}, δc_{55}, δc_{11} and δc_{13} respectively. These analytic results are derived with Born approximation and long wavelength approximation. The analytic scattering patterns are overlain by numerical modelling results for comparison. We observe essential consistency between the two. Perturbations associated with different elastic constants produce different scattering patterns. In angle regimes where the scattering pattern of one parameter is indistinguishable from that of another, the influences of the two parameters are not separable, and cross-talk appears. In Figure 1 we observe that, for instance, the cross-talk between c_{33} and c_{13} at near offset will be strong. We can only record strong wavefields response due to δc_{11} at large offset. Thus, it will be difficult to recover c_{11} and c_{13} for reflection acquisition.

To examine the ability of multi-parameter approximate Hessian to suppress cross-talk, we enact a Gauss-Newton update on a 2D HTI point scatterer model. The model consists of 900 nodes ($N_x = N_z = 30$) with grid size of 5 m in both horizontal and vertical dimensions. The true model is built by embedding one HTI point anomaly at the center position of the background model. Figure 2 shows the multi-parameter approximate Hessian $\tilde{\mathbf{H}}$ (equation (9)), which is a 3600×3600 square and symmetric matrix with 4 diagonal blocks and 12 off-diagonal blocks. It can be seen that the diagonal block $\tilde{\mathbf{H}}_{3333}$ dominates the whole matrix. This is because c_{33} is directly related to P-wave velocity α ($c_{33} = \rho\alpha^2$) and the partial derivative wavefields caused by δc_{33} recorded at the receivers are much stronger than those due to other elastic constants. The 4 diagonal blocks $\tilde{\mathbf{H}}_{3333}$, $\tilde{\mathbf{H}}_{5555}$, $\tilde{\mathbf{H}}_{1111}$ and $\tilde{\mathbf{H}}_{1313}$ are shown in Figures 3a, b ,c and d respectively. The energy distribution in the 4 diagonal blocks are determined by the scattering patterns. The diagonal elements in the diagonal blocks $\tilde{\mathbf{H}}_{3333}$, $\tilde{\mathbf{H}}_{5555}$, $\tilde{\mathbf{H}}_{1111}$ and $\tilde{\mathbf{H}}_{1313}$ are mainly responsible for removing geometrical spreading (Pan et al., 2014b,c), as shown in Figures 4a, b, c and d. The cross-talk between different elastic constants are presented by the 12 off-diagonal blocks of Figure 2. Stronger amplitude in the off-diagonal blocks means stronger cross-talk. Figures 4e, f, g, h, i, and j show the diagonal elements of the off-diagonal blocks $\tilde{\mathbf{H}}_{3355}$, $\tilde{\mathbf{H}}_{3311}$, $\tilde{\mathbf{H}}_{3313}$, $\tilde{\mathbf{H}}_{5511}$, $\tilde{\mathbf{H}}_{5513}$ and $\tilde{\mathbf{H}}_{1113}$ respectively. The data residual vector $\Delta\mathbf{d}_{33}$ caused

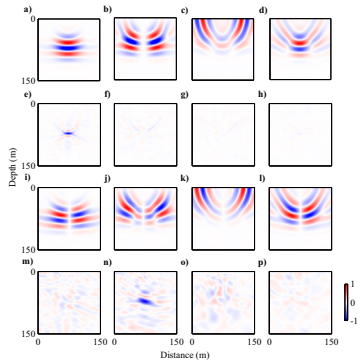

Figure 5: The estimated model perturbations with and without Gauss-Newton approximate Hessian preconditioning.

by δc_{33} is used to construct the gradient vectors $\mathbf{g}_{33}$, $\mathbf{g}_{55}$, $\mathbf{g}_{11}$ and $\mathbf{g}_{13}$, as shown in Figures 5a, b c and d. Only the gradient vector $\mathbf{g}_{33}$ is real and other gradient vectors are cross-talk artifacts. Figures 5e, f, g and h show the estimated model perturbations $\delta\mathbf{c}_{33}$, $\delta\mathbf{c}_{55}$, $\delta\mathbf{c}_{11}$ and $\delta\mathbf{c}_{13}$ with multi-parameter approximate Hessian preconditioning. Figures 5i, j, k and l show the gradient vectors constructed with $\Delta\mathbf{d}_{55}$. Figures 5m, n, o and p show the model perturbation estimations with multi-parameter approximate Hessian preconditioning. It can be seen that the gradient vectors $\mathbf{g}_{33}$ in Figure 5e and $\mathbf{g}_{55}$ in Figure 5n have been resolved greatly. The cross-talk artifacts in other gradient vectors have been suppressed obviously.

Correlating the doubly-scattered energy in the data residuals with the Fréchet derivative wavefields produces artifacts in the gradient. The second-order term $\tilde{\mathbf{H}}$ can mitigate these second-order scattering artifacts. To examine this, two HTI point anomalies are embedded in an isotropic-elastic background model at $\mathbf{r}_1$ (row 17 and column 13) and $\mathbf{r}_2$ (row 19 and column 15). At position $\mathbf{r}_1$, the elastic constants c_{33}, c_{55}, c_{11} and c_{13} are perturbed by $+30\%$, $+10\%$, 0% and $+10\%$. At position $\mathbf{r}_2$, the 4 elastic constants are perturbed by -30%, -10%, -10% and 0%.

Figure 6 shows the elements of first-order and second-order terms plotted in model dimension. Considering the model parameter position $\mathbf{r}_2$, the correlation of the Fréchet derivative wavefields due to $\delta c_{33}(\mathbf{r}_2)$ with the partial derivative wavefields due to $\delta c_{33}(\tilde{\mathbf{r}})$ ($\tilde{\mathbf{r}}$ indicate all positions in the model) forms the 555th row in diagonal block $\tilde{\mathbf{H}}_{3333}$, as shown in Figure 6a. Figures 6b, c and d show the 555th rows in the off-diagonal blocks $\tilde{\mathbf{H}}_{3355}$, $\tilde{\mathbf{H}}_{3311}$ and $\tilde{\mathbf{H}}_{3313}$ respectively. The first-order scattered wavefields due to $\delta c_{33}(\mathbf{r}_2)$ can be further scattered due to $\delta c_{33}(\tilde{\mathbf{r}})$ or $\delta c_{55}(\tilde{\mathbf{r}})$, $\delta c_{11}(\tilde{\mathbf{r}})$ and $\delta c_{13}(\tilde{\mathbf{r}})$. Correlating the second-order scattered wavefields vectors with the data residuals forms the 555th rows of diagonal block $\tilde{\mathbf{H}}_{3333}$ or off-diagonal blocks $\tilde{\mathbf{H}}_{3355}$, $\tilde{\mathbf{H}}_{3311}$ and $\tilde{\mathbf{H}}_{3313}$, as shown in Figure 6e, f, g and h, which are obtained using explicit perturbation method (Pratt et al., 1998). Figure 6i, j, k and l show the 555th rows in blocks $\tilde{\mathbf{H}}_{3333}$, $\tilde{\mathbf{H}}_{3355}$, $\tilde{\mathbf{H}}_{3311}$ and $\tilde{\mathbf{H}}_{3313}$ calculated using adjoint-state method following equation (16).

Finally, we apply the Gauss-Newton and Full-Newton multi-parameter FWI on a more complex two-block-layer model. The initial model is elastic and isotropic. Two anisotropic block layers are embedded in the isotropic background and the true perturbations for elastic constants c_{33}, c_{55}, c_{11} and c_{13} are shown in Figures 7a, b, c and d. Ten iterations are used for inversion with Gauss-Newton and Full-Newton methods. A multi-scale approach is also employed by increasing the frequency band from $[1\text{ Hz}, 10\text{ Hz}]$ to $[1\text{ Hz}, 19\text{ Hz}]$ by 1 Hz every iteration. Figures 7e, f, g and h show the inverted model perturbations for

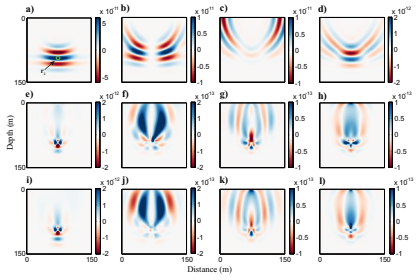

Figure 6: (a), (b), (c) and (d) show the 555th rows in $\tilde{\mathbf{H}}_{3333}$, $\tilde{\mathbf{H}}_{3355}$, $\tilde{\mathbf{H}}_{3311}$, and $\tilde{\mathbf{H}}_{3313}$. (e), (f), (g) and (h) shows the 555th rows in $\tilde{\mathbf{H}}_{3333}$, $\tilde{\mathbf{H}}_{3355}$, $\tilde{\mathbf{H}}_{3311}$, and $\tilde{\mathbf{H}}_{3313}$. (i), (j), (k) and (l) are the results calculated using adjoint-state method.

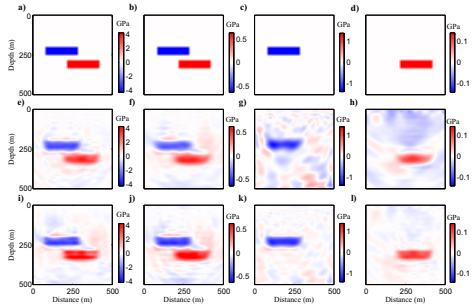

Figure 7: Inversion results comparison. (a), (b), (c) and (d) show the true model perturbations. (e), (f), (g) and (h) show the inverted model perturbations using Gauss-Newton method. (i), (j), (k) and (l) show the inverted model perturbations using Full-Newton method.

the corresponding elastic constants using the Gauss-Newton method. Figures 7i, j, k and l show the inverted model perturbations for the elastic constants using the Full-Newton method. It can be seen that for $\delta\mathbf{c}_{33}$ and $\delta\mathbf{c}_{55}$ (Figures 7e and f), Gauss-Newton method can get acceptable results. While for $\delta\mathbf{c}_{11}$ and $\delta\mathbf{c}_{13}$ (Figures 7g and h), the estimated model perturbations are contaminated by strong artifacts. For Full-Newton method, the inverted elastic constants perturbations are much better and the artifacts in $\delta\mathbf{c}_{11}$ and $\delta\mathbf{c}_{13}$ have been suppressed.

CONCLUSIONS

In this paper, we examine the simultaneous strategies for estimating the elastic constants in HTI media using Gauss-Newton and Full-Newton multi-parameter FWI. We discuss the role of multi-parameter Hessian in mitigating cross-talk and suppressing second-order scattering effects. Full-Newton method shows better performance than Gauss-Newton method with a two-block-layer model.

ACKNOWLEDGMENTS

This research was supported by the Consortium for Research in Elastic Wave Exploration Seismology (CREWES) and National Science and Engineering Research Council of Canada (NSERC, CRDPJ 379744–08). The authors thank to the researchers Di Yang, Sam Ahmad Zamanian, Xuan Feng, Sudhish Bakku, and Stephen Brown at MIT-ERL for their valuable discussions and suggestions.